Enhancing the Capacity of the Indoor 60 GHz Band Via Modified Indoor Environments Using Ring Frequency Selective Surface Wallpapers and Path Loss Models

Nidal Qasem

Department of Electronics and Communications Engineering, Al-Ahliyya Amman University, Jordan

Article Info	ABSTRACT
	The 60 GHz band has been selected for short-range communication systems to meet consumers' needs for high data rates. However, this frequency is attenuated by obstacles. This study addresses the limitations of the 60 GHz band by modifying indoor environments with ring Frequency Selective Surfaces (FSSs) wallpaper, thereby increasing its utilization. The ring FSS wallpaper response at a 61.5 GHz frequency has been analyzed using both MATLAB and Computer Simulation Technology (CST) Microwave Studio (MWS) software. 'Wireless InSite' is also used to demonstrate enhanced wave propagation in a building modified with ring FSSs wallpaper. The demonstration is applied to Single Input Single Output (SISO) and Multiple Input Multiple Output (MIMO) systems to verify the effectiveness of FSSs on such systems' capacity. The effectiveness of the suggested modification over delay spread has been studied for the MIMO scenario, as well as the effect of the human body on capacity. Simulation results presented here show that modifying a building using ring FSS wallpaper is an attractive scheme for significantly improving the indoor 60 GHz wireless communications band. This paper also presents and compares two large-scale indoor propagation Path Loss Models (PLMs), the Close-In (CI) free space reference distance model and the Floating Intercept (FI) model. Data obtained from 'Wireless InSite' over distances ranging from 4 to 14.31 m is analyzed. Results show that the CI model provides good estimation and exhibits stable behavior over frequencies and distances, with a solid physical basis and less computational complexity when compared to the FI model.

Corresponding Author:

Nidal Qasem,
Department of Electronics and Communications Engineering, Faculty of Engineering,
Al-Ahliyya Amman University,
Zip-code (Postal Address): 19328, Amman, Jordan.
Email: Ne.qasem@ammanu.edu.jo

1.   INTRODUCTION

The 60 GHz band is a perfect choice for achieving the desired goal of obtaining high-speed data rates with a theoretical upper limit of 6.5 Gigabit-per-second (Gbps). It also provides benefits, such as a 10 W maximum transmit power, a high level of frequency reuse, and a high level of savings in operations [1]. When comparing the 60 GHz band with other unlicensed bands, it can be seen that the 60 GHz band provides much higher data rates. However, it is easily blocked by obstacles, and this places more restrictions on using it. For example, concrete materials, glass, walls, and the human body can cause large signal attenuation on a 60 GHz band. Thus, the 60 GHz communication band is more suitable for indoor and short-range environments in which sufficient reflectors are present [2].

The unlicensed 60 GHz band allocates 9 GHz sub-bands, which varies slightly depending on local regulations. Technical standards divide this band into four 2.16 GHz channels. The 61.5 GHz frequency which allocates at the second channel has been selected for this study since it is commonly used as an unlicensed frequency in different regions and countries [3]. Indoor channel simulations/measurements are vital to understanding Path Loss (PL) as a function of distance, and temporal and spatial characteristics, which are crucial in performing system-wide simulations to estimate network system capacities and overall data throughputs. PL models (PLMs) are very important models with which to comprehend and study the attenuation of signal propagation from transmitters (Tx's) to receivers (Rx's), and allow accurate channel models to be designed for network simulations, which, in turn, help in designing communication systems. The most common single-frequency PLMs are Close-In (CI) and Floating Intercept (FI). Both of these models will be studied in this paper [4].

This study focuses on utilization by suggesting an unprecedented technique that can control the propagation of the indoor wireless environment of the 60 GHz band by completely reflecting the entire 60 GHz band, keeping it inside the area of interest. This technique uses ring Frequency Selective Services (FSSs) wallpaper in order to provide a more strongly received signal; it does this by increasing the multipath propagation due to the variety of signal paths. In addition, this research provides a comprehensive study of indoor propagation at the 60 GHz band by using different scenarios to generate a large-scale Path Loss Model (PLM) for enhancing 5th generation standards at the 60 GHz band. In any case, extensive indoor propagation simulations at the 60 GHz band are needed in order to accurately characterize and model the channel needed to design a capable indoor system at this frequency.

This paper is organized as follows: Section 2 explains the Equivalent Circuit Model (ECM) analysis technique and applies it to the ring FSS wallpaper. Next, Section 3 is divided to subsections. First, it examines the simulation results and discussion. It starts with ring FSS wallpaper, and its transmission and reflection coefficients, using both MATLAB and Computer Simulation Technology (CST) Microwave Studio (MWS). Then, demonstrates investigations of some selected scenarios using 'Wireless InSite', these scenarios have been tested in both the Single Input Single Output (SISO) and Multiple Input Multiple Output (MIMO) cases. SISO and MIMO scenarios are presented and performed both with and without ring FSS wallpaper to investigate ring FSS wallpaper's effect on the received signal power, both in the presence and absence of human bodies. Also, it presents the SISO and MIMO capacity enhancement results. In addition, it explains the delay spread calculations and results. As well as, it explains and presents PLMs results. Finally, Section 4 concludes this paper.

2.   RING FSS WALLPAPER

FSSs are planar periodic structures that can be used as a filter for a specific frequency of electromagnetic waves, depending on the interference caused by the periodic arrays of both dielectric and conducting materials which makes a frequency selective response [5], [6]. FSSs, in general, have many common shapes and geometries, such as a square loop, ring, dipole, cross dipole, Jerusalem cross, and tripole. These types can be in one of four modes; high-pass, low-pass, band-pass, and band stop filter [7].

Previous research shows that the ring FSS wallpaper frequency response characteristics provide excellent performance; angular sensitivity, cross polarization, bandwidth, and small band separation [8]. Thus, the ring FSS shape has been selected for this study. Ring FSS is a circular conductive material placed on a dielectric surface used as a band-stop filter, which is an excellent reflector for a resonant frequency. Ring FSS physical parameters are shown in Figure 1.
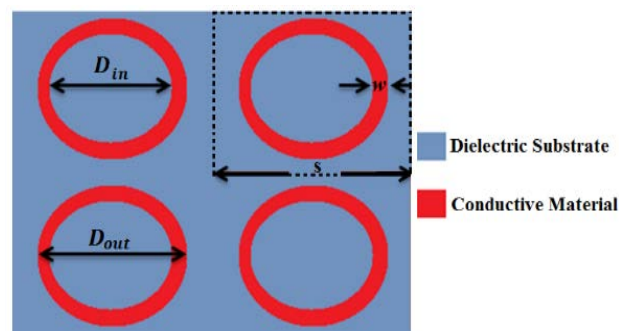
Figure 1. Array of ring FSS elements.

In this Figure, w is the width of the conductive ring, D_{out} is the outer diameter of the ring, D_{in} is the inner diameter of the ring, s is the separation period between FSS elements, and h is the substrate thickness. In order to test the response of the designed ring FSS, the ECM analysis technique has been used. This technique depends on the idea that the interaction between the wave and the FSS is identically the same as a wave that passes through a transmission line with shunt lumped circuit impedances, as shown in Figure 2(b).

(a) Ring FSS.   (b) ECM.
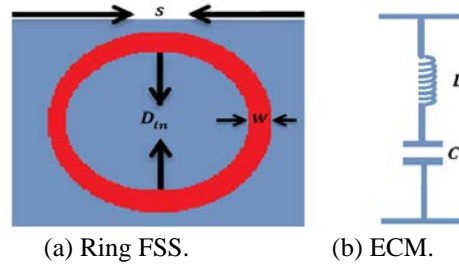
Figure 2. Ring FSS and its equivalent circuit

The ECM method has been used to extract the circuit lumped parameters capacitance (C) and inductance (L), depending on the FSS physical parameters; D_{in}, D_{out}, w, and s, as depicted in Figure 2(a). To find the ring size, D_{out} is determined depending on the basic ring resonator equation [9]:

$$D_{out} = \frac{\lambda_o}{\pi * \sqrt{\varepsilon_{eff}}} \tag{1}$$

where λ_o is the wavelength at the selected resonant frequency, and [9]:

$$\varepsilon_{eff} = \frac{\varepsilon_r + \varepsilon_o}{2} \tag{2}$$

Where ε_r and ε_o are relative permittivity values for the dielectric substrate and the free space, respectively. The s must be less than the shortest wavelength in the operating band, and the values of D_{in} and h can be determined empirically to achieve the best response. Finally, the value of w can be determined using the following equation [9]:

$$w = \frac{D_{out} - D_{in}}{2} \tag{3}$$

A set of optimal values, based on trials, used in this study are presented in Table 1.

Table 1. The Physical Parameters Used for Designing Ring FSS.

Resonant Frequency	61.5 GHz
λ_o	5 mm
D_{out}	1.1 mm
D_{in}	1.07 mm
w	0.015 mm
h	0.1 mm

Depending on the selected physical parameters above, the inductance of the ring resonator can be calculated using the equation [10]:

$$L(nH) = 39.37 \frac{a^2}{8a + 11q} * K_g \tag{4}$$

Factors (a) and (q) are in mm, where [10]:

$$a = \frac{D_{out} + D_{in}}{4} \tag{5}$$

and

$$q = \frac{D_{out} - D_{in}}{2} \tag{6}$$

K_g is the correction term, which takes into consideration the effect of the ground plane. The correction term decreases the value of the inductance by getting nearer to the ground, depending on the following relation [9]:

$$K_g = 0.57 - 0.145 \ln \frac{w}{h} \tag{7}$$

and the capacitance of the ring FSS is [9]:

$$C(pF) = \frac{1}{(2\pi f)^2} - \frac{1}{L} \tag{8}$$

After calculating the equivalent inductance and capacitance, the ABCD matrix has been used [2]. The transmission lines that can represent the ABCD matrix are shown in the Figure 3.
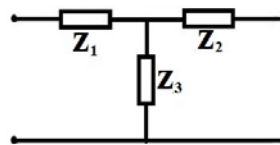
Figure 3. Transmission line, which can be represented by an ABCD matrix

The ABCD matrix can be expressed as a function of the transmission coefficient (S_{21}) and reflection coefficient (S_{11}) [2]:

$$S_{21} = T = \frac{2}{A+B+C+D} = \frac{2}{1+0+\frac{1}{Z_3}+1} = \frac{2}{2+\frac{1}{Z_3}} = \frac{2}{2+Y} \tag{9}$$

$$S_{11} = \Gamma = 1 - |T|^2 = 1 - \frac{4}{4+Y^2} \tag{10}$$

3. RESULTS AND DISCUSSION
3.1. Ring FSS (MATLAB)

MATLAB has been used to solve the theoretical equations for ECM for the suggested design of the ring FSS element. The basic rule of thumb in designing ring circumference is to make its response approximately equal to the resonant frequency (61.5 GHz). Figures 4 and 5 show the S_{21} and S_{11} responses coefficients for the designed ring FSS at a 0° incidence angle, respectively.
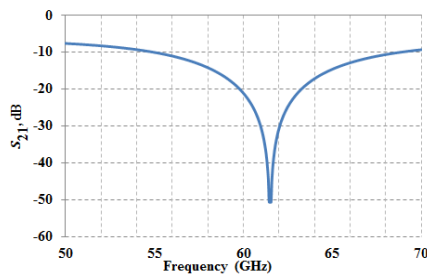
Figure 4. The theoretical frequency transmission response of ring FSS wallpaper based on ECM equations
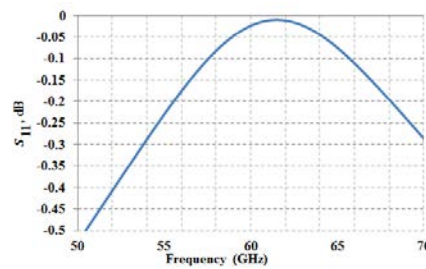
Figure 5. The theoretical frequency reflection response of ring FSS wallpaper based on ECM equations

3.2. Ring FSS (CST-MWS)

CST-MWS is used to test and analyse the designed ring FSS parameters. The analysis method used is the finite integration technique on Cartesian or tetrahedral grids [11]. Ring FSS wallpaper has been tested for a range of different incidence angles from 0° to 60°. The S21 is presented for both Transverse Electric (TE) and Transverse Magnetic (TM) modes, as shown in Figures 6 and 7, respectively. The S_{11} is also presented for the TE and TM modes, as shown in Figures 8 and 9, respectively. All of the following figures for the transmission and reflection coefficients are expressed in a range of frequencies from 50 to 70 GHz. Copper with a 0.07 mm thickness is used as the conductive material. The dielectric material is Arlon AD 300, which has a 0.1 mm thickness and a relative permittivity value of 3.
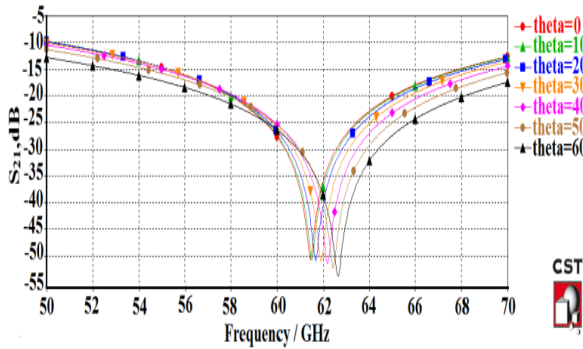
Figure 6. The transmission response of ring FSS wallpaper for TE-mode
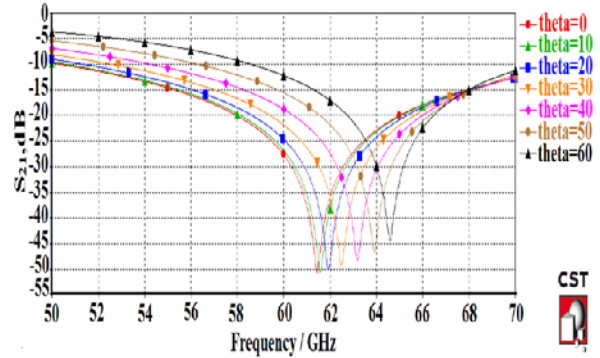
Figure 7. The transmission response of ring FSS wallpaper for TM-mode
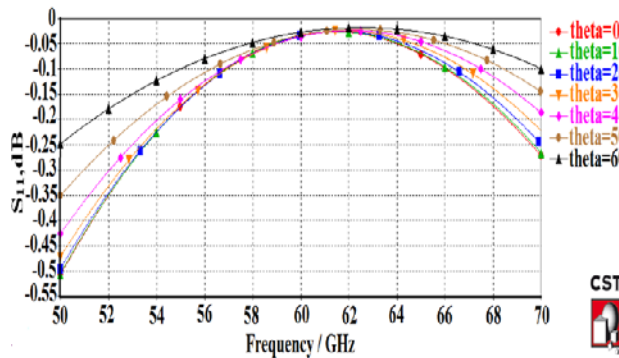
Figure 8. The reflection response of ring FSS wallpaper for TE-mode
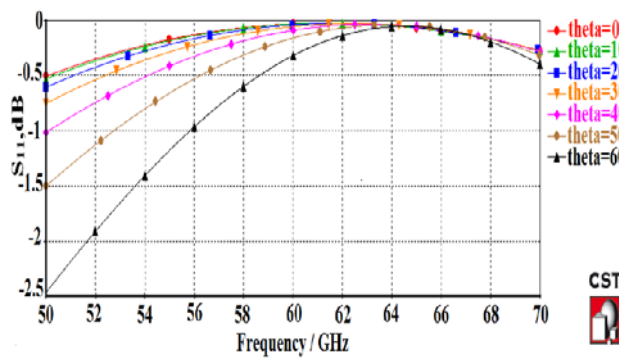
Figure 9. The reflection response of ring FSS wallpaper for TM-mode

In order to evaluate the response of a filter as a band-stop, the attenuation value must exceed -25 dB at the resonant frequency (61.5 GHz) to kill the signal [12]. As shown in Figures 6 and 7, the transmission coefficients for both TE and TM modes are more than -25 dB. That means that the signal will be dead when trying to penetrate the area of interest. The reflection coefficients shown in Figures 8 and 9 are also smaller than -0.05 dB at 61.5 GHz, which allows the ring FSS wallpaper to act as a perfect reflector inside the area of interest, achieving its goal. Figure 10 shows how the designed ring FSS wallpaper attenuates the waves of 61.5 GHz from port 1 to port 2. Figure 11 shows how the designed ring FSS wallpaper allows the waves of 5 GHz to propagate without attenuation from port 1 to port 2.
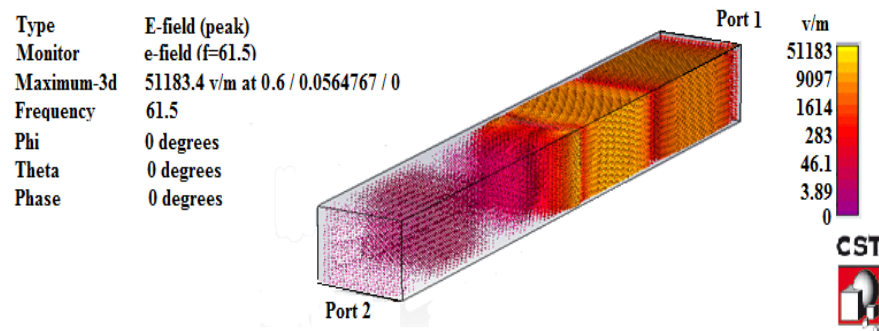
Figure 10. Signal propagation animation snapshot, from port 1 to port 2, at 61.5 GHz frequency
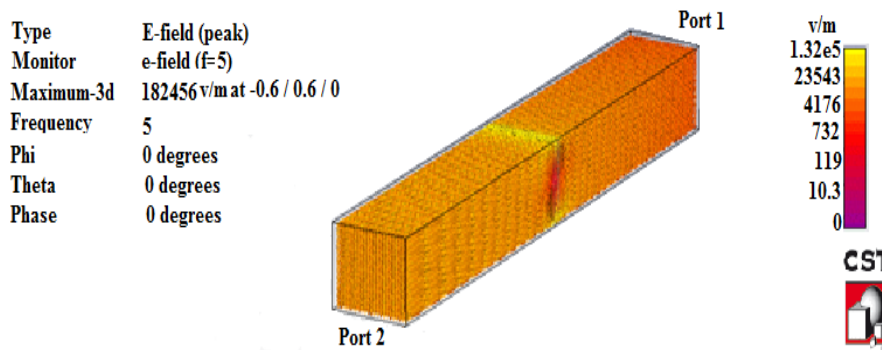
Figure 11. Signal propagation animation snapshot, from port 1 to port 2, at 5 GHz frequency

3.3. Investigation of Scenarios Using 'Wireless InSite'

'Wireless InSite' is used as a tool to evaluate the received power for different scenarios inside the area of interest [13]. The reflection and transmission coefficient values of the ring FSS wallpaper have been exported to 'Wireless InSite' in order to obtain the ring FSS wallpaper response. Two scenarios in a room with dimension 15×10 m have been investigated. The first scenario investigates a SISO communication system, in the case of presence and absence of ring FSS. The second scenario investigates a MIMO communication system, while MIMO scenario studies two more sub-scenarios; with and without human body.

3.3.1. SISO System Scenario

This scenario consists of a SISO system with a single Tx and 20 Rx's situated in different locations. The Tx has a directional antenna with 10 dBm input power, 14 dBi gain, 2.5 m height, and 90° Half-Power Beam Width (HPBW). Each Rx has an omnidirectional antenna with a height of 1.5 m and a sensitivity of -64 dBm, which satisfies the required Gbps data rate (2 Gbps) [1]. The 2D view of this scenario is shown in Figure 12.
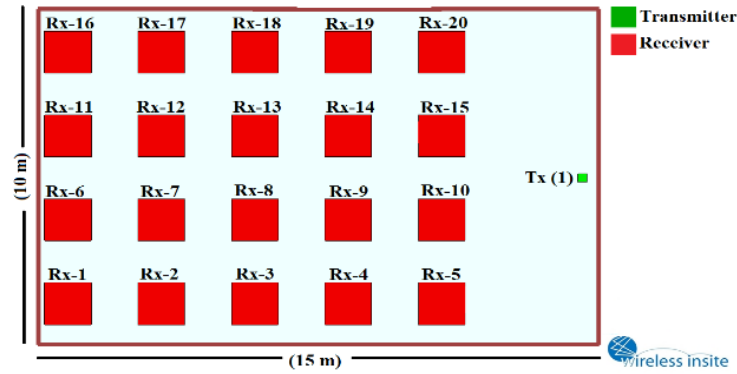
Figure 12. 2D view of the area of interest

Table 2 shows the electrical parameters of the materials used in this study [13]. Figure 13 shows the 3D view of the first scenario, which has been studied without using ring FSS wallpaper. The received signal power at each Rx location is shown in Figure 14.

Table 2. Electrical Parameters Used for Building Area of Interest [13]

Component	Material	Conductivity, σ (S/m)	Relative Electrical Permittivity, ε_r	Thickness (m)
Walls	Brick	0.001	4.44	0.150
Ceiling and Floor	Concrete	0.015	15	0.3
Windows	Glass	0	2.4	0.003
Doors	Wood	0	5	0.03
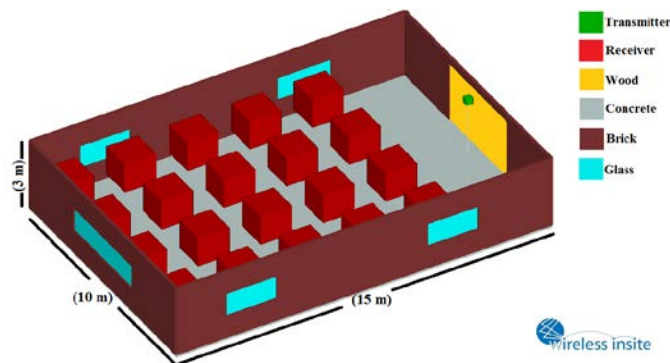
Figure 13. 3D view for the SISO scenario without ring FSS wallpaper
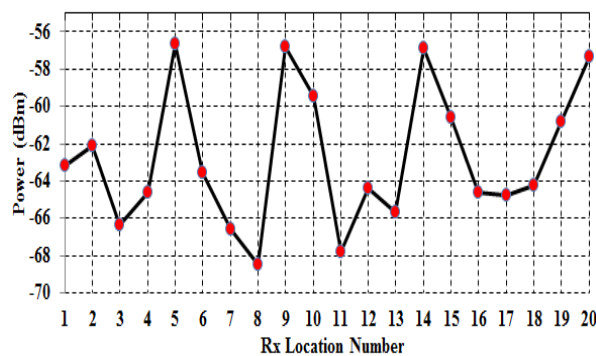
Figure 14. The received signal power for each Rx location number for the SISO system scenario without ring FSS wallpaper

Ring FSS wallpaper has been attached a distance of λ/10 away from the wall to eliminate the coupling effect issues [7], as shown in Figure 15. In this case, ring FSS wallpaper represents an excellent reflector for the 60 GHz band, which will increase the multipath propagation in the area of interest as well as increase the strength of the received signal power. Figure 16 shows the received signal power at each Rx location.
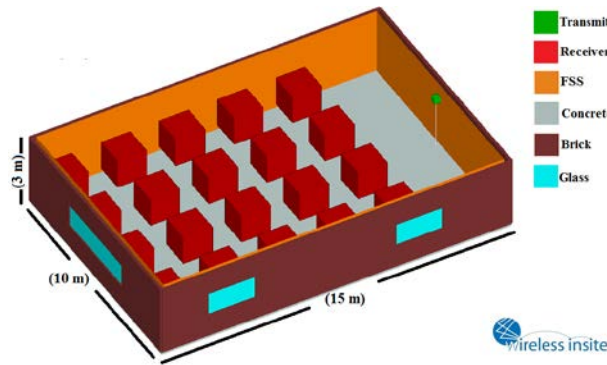
Figure 15. 3D view for the SISO scenario with ring FSS wallpaper
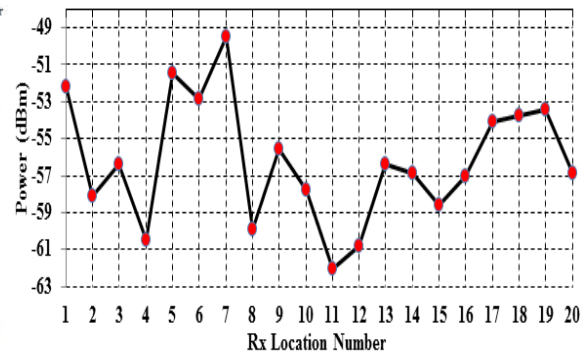
Figure 16. The received signal power for each Rx Location Number for the SISO scenario with FSS

Figure 17 shows the difference of the received signal power between SISO system cases before and after attaching ring FSS wallpaper at each Rx location number. Figure 17 shows that the received power has been enhanced after attaching ring FSS wallpaper by an average of 6.45 dB.
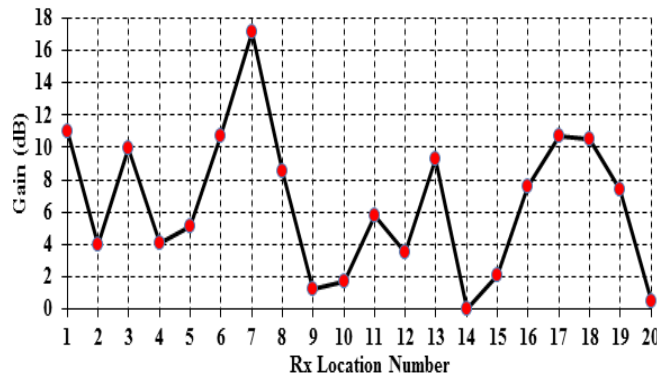
Figure 17. The gain enhancement for each Rx location number for SISO system scenario with/without ring FSS wallpaper

3.3.2. MIMO System Scenario
3.3.2.1. MIMO without Ring FSS Wallpaper

This scenario contains a 2x2 MIMO communication system for Tx and the Rx's. Both the Tx and Rx's are assumed to consist of two antenna elements spaced by λ/2 [14]. Tx has a directional antenna with 10 dBm input power, 14 dBi gain, 2.5 m height, and 90° HPBW. Rx's are distributed in 20 locations. Each Rx has an omnidirectional antenna with a sensitivity of -64 dBm and a 1.5 m height.

a.   Without human bodies

The 2D and 3D views of this scenario are shown in Figures 18 and 19. Figure 20 shows the received signal power at each Rx location.
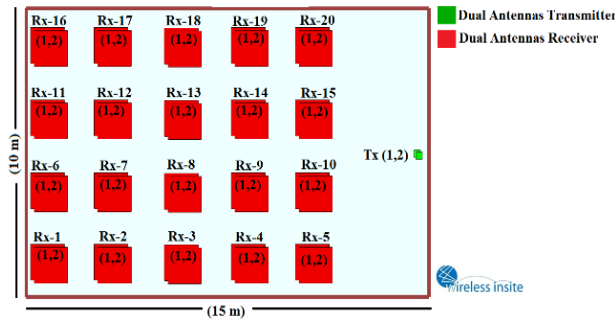
Figure 18. 2D view for the MIMO scenario
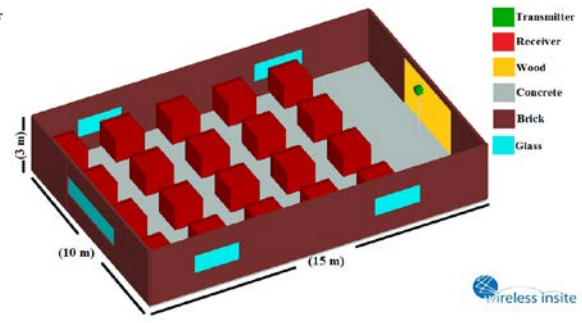
Figure 19. 3D view for the MIMO scenario without ring FSS wallpaper and human bodies
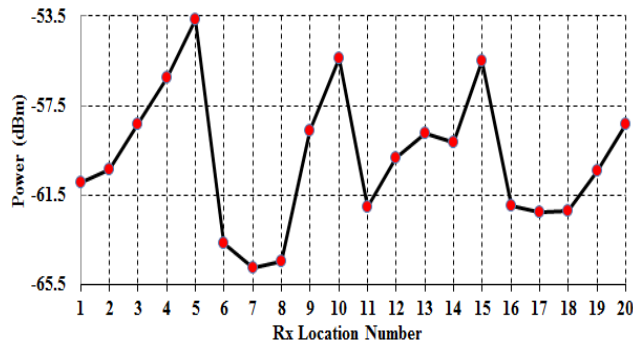
Figure 20. The received signal power for each Rx location number for the MIMO system scenario without ring FSS wallpaper and human bodies

b.   With human bodies

The 2D and 3D views of this scenario are shown in Figures 21 and 22. The black parallelepipeds represent the number of human bodies situated randomly in the room. The human body has been modelled inside 'Wireless InSite' based on the complex permittivity values of its basic components; skin, fat, muscle, and pure water, at a 60 GHz resonant frequency, as summarized in Table 3 [2]. The received power at each Rx location is shown in Figure 23. Figure 24 shows that the average received power in the MIMO system has been attenuated by 3 dB, on average, with the presence of human bodies.

Table 3. Complex Permittivity at 60 GHz of Human Body Components

Human Tissues	ε_c
Skin	$7.98 - j10.91$
Fat	$2.51 - j0.84$
Muscle	$12.85 - j15.74$
Pure Water (20° C)	$11.9 - j19.5$
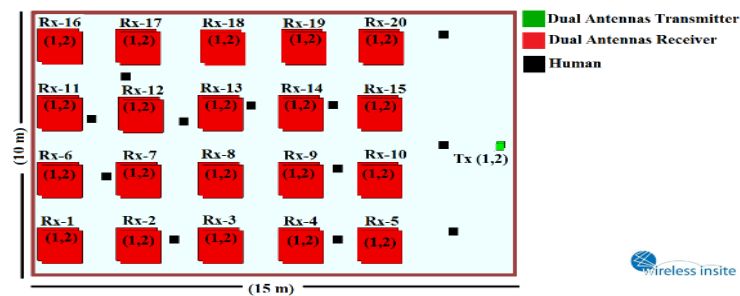
Figure 21. 2D view for the MIMO scenario without ring FSS, but with a number of human bodies
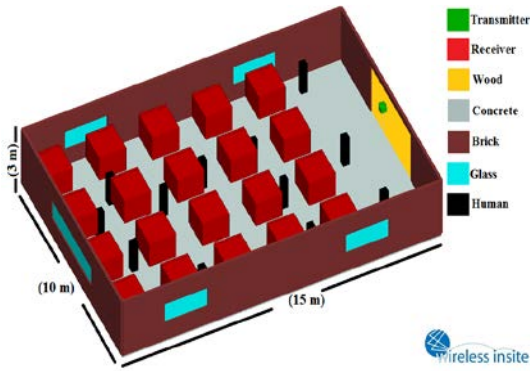
Figure 22. 3D view for the MIMO scenario without ring FSS wallpaper, but with a number of human bodies
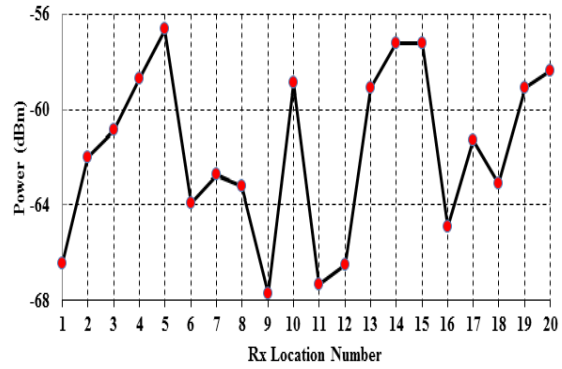
Figure 23. The received signal power for each Rx location number for the MIMO system scenario without ring FSS wallpaper, but with a number of human bodies
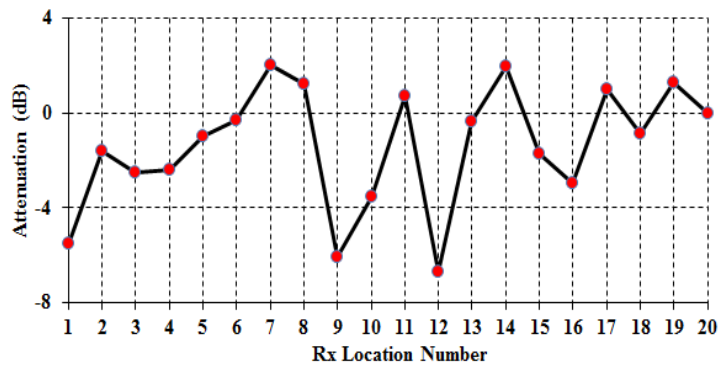
Figure 24. The received signal power for each Rx location number for the MIMO system scenario without ring FSS wallpaper, but with a number of human bodies

3.3.3. MIMO with Ring FSS Wallpaper
a. Without human bodies

The same scenario used in Section 3.3.2.1 is repeated by attaching ring FSS wallpaper λ/10 away from the wall, as shown in Figure 25. Figure 26 shows the received signal power at each Rx location.
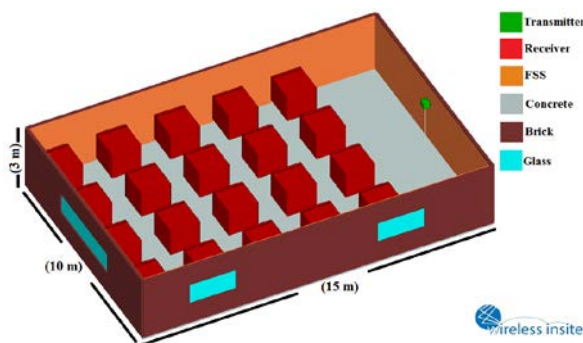
Figure 25. 3D view for the MIMO scenario with ring FSS wallpaper, but without human bodies
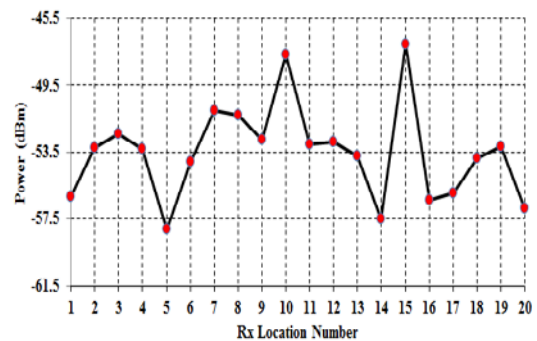
Figure 26. The received signal power for each Rx location number for the MIMO system scenario with ring FSS wallpaper, but without human bodies

b.   With human bodies

Figure 27 shows the above scenario with a number of human bodies added. Figure 28 shows the received signal power at each Rx location. Figure 29 shows that the received power has been reduced in the MIMO system scenario with ring FSS wallpaper and a number of human bodies by an average of 2 dB compared to the scenario without human bodies.
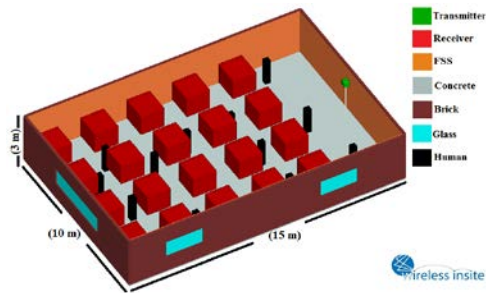
Figure 27. 3D view for the MIMO scenario with ring FSS wallpaper and a number of human bodies
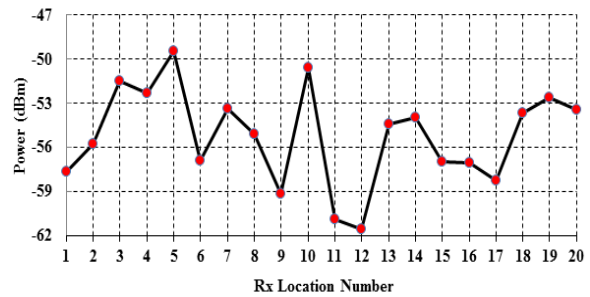
Figure 28. The received signal power for each Rx location number for the MIMO system scenario with ring FSS wallpaper and a number of human bodies
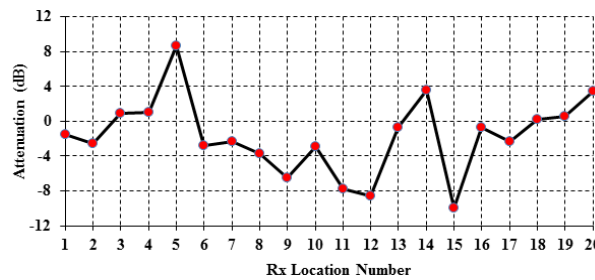
Figure 29. The achieved attenuation for each Rx location number for MIMO system scenario with ring FSS wallpaper with/without human bodies

Figures 30 and 31 show the difference in the received signal power before and after attaching ring FSS wallpaper at each Rx location for the MIMO system scenario with/without human bodies, respectively. In these figures, the received power at each Rx location has been enhanced after attaching ring FSS wallpaper by an average of 6.87 with and 6.53 dB without human bodies. Note that the received power at Rx location number 5, as seen in Figure 30, has been attenuated due to the beam-width of the Tx, whose signal suffers more reflections before reach the Rx.
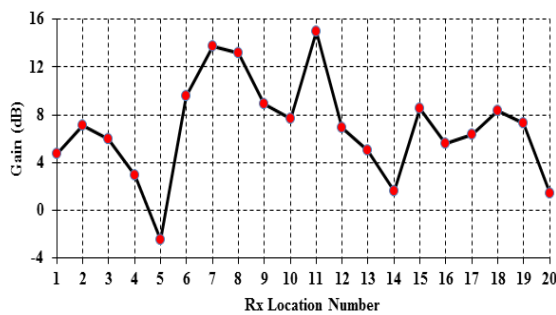
Figure 30. The gain enhancement for each Rx location number between MIMO system scenarios with/without ring FSS wallpaper without human bodies
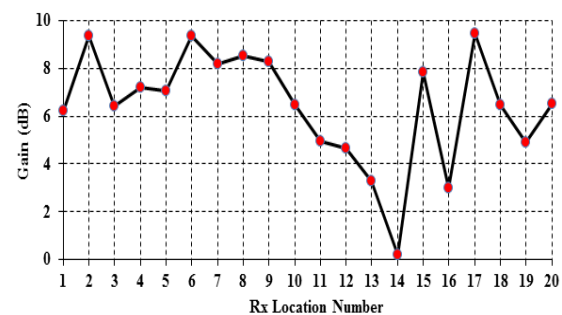
Figure 31. The gain enhancement for each Rx location number between MIMO system scenarios with/without ring FSS wallpaper without human bodies

3.4. SISO and MIMO Systems Capacity

In order to evaluate the response for the scenarios above, the capacity metric is studied. The capacity of the SISO system can be calculated using the following equation [15], [16]:

$$C_{SISO} = \log_2(1 + SNR) \tag{11}$$

where SNR is the Signal to Noise Ratio. Also, the formulation for the 2x2 MIMO model used to determine the capacity is as follows [15]-[17]:

$$C_{MIMO} = \log_2 det\left(I + \frac{SNR}{n}HH^T\right) \tag{12}$$

where det is the determinant, I is the 2×2 identity matrix, n is the number of antennas used (2 in this case), H is the channel matrix, and H^T is the channel conjugate-transpose matrix. H can be determined by the sum of all rays arriving at each Rx antenna and is computed by the following formula [15]:

$$h_{ij} = \sum_{k=1}^{M} \sqrt{P_k} \cdot e^{i(2\pi/\lambda)l_k} \cdot e^{i2\pi f_0 T_k} \tag{13}$$

where M is the number of received rays, P_k is the received power, l_k is the length of the kth ray, f_0 is the carrier frequency, and T_k is the time delay of the kth ray. P_k, l_k, and T_k are obtained from 'Wireless InSite'. Figures 32 and 33 show the capacity of all of the SISO and MIMO scenarios.
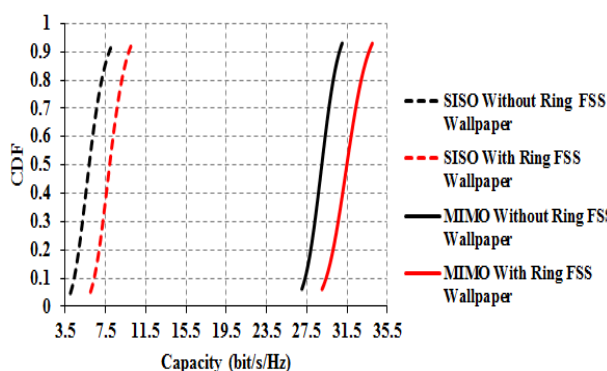
Figure 32. A Cumulative Distribution Function (CDF) plot showing the comparison between SISO and MIMO systems with and without ring FSS wallpaper for 60 GHz band
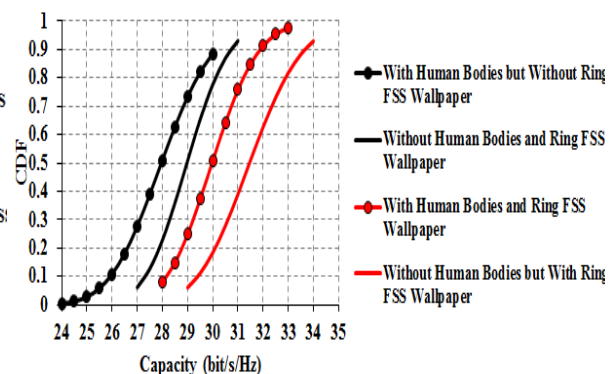
Figure 33. A CDF plot showing the comparison in the MIMO system between the presence and absence of human bodies, and with/without ring FSS wallpaper for a 60 GHz band

Figures 32 and 33 show clearly that the capacity has been increased for both the SISO and MIMO systems after attaching ring FSS wallpaper inside the area of interest. Figure 32 shows that the MIMO system capacity has been enhanced by 24 bit/s/Hz compared to the SISO system per median reading. The presence of human bodies affects the strength of the received signal and decreases the capacity by an average of 1.25 bit/s/Hz, as shown in Figure 33. Using ring FSS wallpaper enhances the capacity by an average of 2.5 bit/s/Hz, which proves that the presence of ring FSS wallpaper in an indoor environment increases the strong reflected wave components in each Rx location. The idea is that the presence of various multipath components at every receiving element would make the channel more Rayleigh (lower K-factor), achieving lower correlation and, hence, higher capacity [7].

3.5. Delay Spread

Delay spread is a statistical measure of the time dispersion of any communication channel that is considered a performance evaluating factor for any communication system [7], [18]. Delay spread is explained in detail mathematically in the following equations [13]:

$$\sigma_{RMS} = \sqrt{\frac{\Sigma_{i=1}^{Np} P_i t_i^2}{P_R} - \bar{t}^2} \tag{14}$$

where σ_{RMS} is the Root Mean Square (RMS) delay spread, P_R is the averaged received power, N_p is the number of paths, P_i is the time averaged power in watts of the ith path, and t_i is the time of arrival [2]:

$$t_i = \frac{L_i}{c} \tag{15}$$

where L_i is the total geometrical path length and c is the speed of light in free space. The mean time of arrival is [13]:

$$\bar{t} = \frac{\Sigma_{i=1}^{Np} P_i t_i}{P_R} \tag{16}$$

The delay spread results for the MIMO system are shown in Figure 34. Depending on the median of delay spread values, as seen in Figure 34, the average delay spread in the presence of ring FSS wallpaper is 14.5 ns, while, in the absence of ring FSS wallpaper, it is 7 ns. These values indicate that the delay spread has been slightly increased by an average of 7.5 ns, which is still within the acceptable range for a 60 GHz band [19].
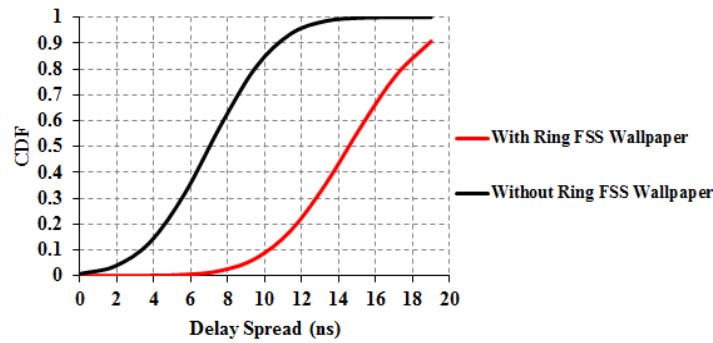
Figure 34. A CDF plot showing the delay spread for the MIMO system for a 60 GHz band

3.6. Large-scale PLMs

Large-scale PLMs estimate the attenuation over distance of propagation signals and are vital for designing communication systems. Different types (deterministic, empirical, and stochastic) of large-scale PLMs exist, but a measurement-based PLM provides realistic insight into the propagation characteristics of a wireless channel [4]. Two types of PLMs are studied in this paper: CI and FI. The CI PLM is defined by the Path Loss Exponent (PLE) n [20], [21]:

$$PL^{CI}(f, d) \, [dB] = FSPL(f, d_o) + 10n\log_{10}\left(\frac{d}{d_o}\right) + X_\sigma^{CI} \tag{17}$$

$$FSPL(f, d_o) = 10\log_{10}\left(\frac{4\pi d_o}{\lambda}\right)^2 \tag{18}$$

where λ is the wavelength in m, $d_o = 1 \, m$, and X_σ^{CI} is a zero mean Gaussian random variable with standard deviation σ^{CI} given by [20]:

$$X_\sigma^{CI} = PL^{CI}[dB] - FSPL(f, d_o)[dB] - 10n\log_{10}(d) = A - nD \tag{19}$$

$$\sigma^{CI} = \sqrt{\Sigma \frac{X_\sigma^{CI2}}{N}} = \sqrt{\Sigma \frac{(A-nD)^2}{N}} \tag{20}$$

where $A = PL^{CI}(f,d)[dB] - FSPL(f,d_o)[dB]$, $D = 10log_{10}(d)$, and N is the number of measured PL data points. The CI PLM uses a physically based reference distance, d_o, and n is the mean PLE, which indicates how fast PL increases with distance. The FI PLM is currently used in standards work, such as the 3rd Generation Partnership Project (3GPP), and can be calculated as follow [22], [23]:

$$PL^{FI}(d)[dB] = \alpha + 10\beta log_{10}d + X_\sigma^{FI} \qquad (21)$$

Assume that $B = PL^{FI}(d)[dB]$ and the zero mean Gaussian random variable is [24]:

$$X_\sigma^{FI} = B - \alpha - \beta D \qquad (22)$$

and the standard deviation σ^{FI} is [24]:

$$\sigma^{FI} = \sqrt{\sum \frac{X_\sigma^{FI2}}{N}} = \sqrt{\sum \frac{(B-\alpha-\beta D)^2}{N}} \qquad (23)$$

where α is the floating intercept and given by [24]:

$$\alpha = \frac{\sum D \sum BD - \sum D^2 \sum B}{(\sum D)^2 - N \sum D^2} \qquad (24)$$

and β is the slope of the line (different than the PLE) and given by [24]:

$$\beta = \frac{\sum D \sum B - N \sum DB}{(\sum D)^2 - N \sum D^2} \qquad (25)$$

where X_σ^{FI} is a log-normal random variable with mean 0 dB and standard deviation σ^{FI}. Using the two large-scale propagation PLMs presented above and the indoor simulation data for a 60 GHz band, PL parameters are analysed and compared. The single-frequency CI and FI PLMs parameters at a 60 GHz band for different indoor scenarios are presented in Table 4 (for the purpose of comparing PLMs and saving space, only directional antenna for Tx and omnidirectional antenna for Rx PL data captured with vertically-polarized (V-V) Tx and Rx antennas are included).

Table 4. Parameters for the single-frequency CI and FI PLMs in a typical modified indoor scenario.

Scenario	Pol.	Freq. (GHz)	Env.	Distance Range (m)	Model	PLE/ β	α [dB]	σ [dB]
Ring FSS Wallpaper with Humans	V-V	61.5	LOS	4-14.31	CI	1.5	-	2.68
					FI	0.79	74.8	2.4
			NLOS	4-14.31	CI	3	-	6.4
					FI	0.79	99	3.2
			NLOS-Best	4-14.31	CI	2.54	-	4.2
					FI	0.33	89	1.8
Ring FSS Wallpaper without Humans	V-V	61.5	LOS	4-14.31	CI	1.46	-	2.2
					FI	0.76	74	2
			NLOS	4-14.31	CI	2.9	-	6.13
					FI	-0.16	98	2.6
			NLOS-Best	4-14.31	CI	2.5	-	4.2
					FI	0.21	90.5	1.2
Humans without Ring FSS Wallpaper	V-V	61.5	LOS	4-14.31	CI	1.76	-	3
					FI	1	75.37	2.74
			NLOS	4-14.31	CI	3.39	-	7.22
					FI	-0.02	101.28	3.87
			NLOS-Best	4-14.31	CI	2.9	-	5.87
					FI	0.15	95	3.34
Without Humans and Ring FSS Wallpaper	V-V	61.5	LOS	4-14.31	CI	1.7	-	2
					FI	1.36	74	2
			NLOS	4-14.31	CI	3.4	-	6.88
					FI	0.01	98	3.5
			NLOS-Best	4-14.31	CI	3	-	5.6
					FI	-0.01	90.5	2.24

It can be observed from Table 4 that the CI model provides intuitive PLM parameter values due to its physical basis, while the parameters in the FI model sometimes contradict fundamental principles. For example, for the humans without ring FSS wallpaper scenario in a Non-Line-Of-Sight (NLOS) environment, the CI model generates a PLE of 3.39, which nearly matches the theoretical free-space NLOS PLE of 4; however, in the FI model, it is -0.02, meaning that the PL decreases with distance, which is obviously not reasonable or physically possible in a passive channel.

The resulting single-frequency PLM parameters emphasize the frequency dependence of indoor PL beyond the first meter of FSPL, where PLEs in the ring FSS wallpaper without humans scenarios at 61.5 GHz are larger than the PLEs for the same scenarios, but without ring FSS wallpaper, as shown in Table 4. Specifically, Line-Of-Sight (LOS) PLEs are 1.46 and 1.7 at 61.5 GHz with/without ring FSS wallpaper in without humans scenarios, respectively, indicating constructive interference and waveguiding effects in LOS indoor channels at mm-wave frequencies. Furthermore, the NLOS PLEs are 3.4 and 2.9 at 61.5 GHz for the same scenarios, respectively, showing that 61.5 GHz propagating waves attenuate by 10 dB more per meter of distance in the indoor environment beyond the first meter, as provided in Table 4. For with/without ring FSS wallpaper with humans scenarios, LOS PLEs are 1.5 and 1.76 at 61.5 GHz, respectively, indicating constructive interference and waveguiding effects in LOS indoor channels at mm-wave frequencies. Furthermore, the same reasons apply to the NLOS PLEs, which are 3 and 3.9 at 61.5 GHz for the same scenarios, respectively. By using the strongest NLOS received power path from Tx-Rx (NLOS-Best) PLE reduced to 2.54 and 2.9, which is an important improvement for NLOS case.

The FI model indicates lower attenuation as a function of log-distance in some cases (human without ring FSS wallpaper LOS $\beta = 1$, compared to $n = 1.76$, and NLOS $\beta = -0.02$, compared to $n = 3.39$). However, the FI model parameters can exhibit strange, non-physics-based values, specifically, when β is negative, which implies ultra-low loss with distance (less than in a waveguide), which does not follow basic physics.

We use $d_o=1\ m$ in mm-wave PLMs since base stations will be shorter or mounted indoors and closer to obstructions [23]. The physically-based 1 m FSPL anchor of the CI model for single-frequencies allows for a simpler model (only one parameter) with virtually no decrease in model accuracy by representing free-space propagation close to the transmitting antenna. Therefore, the more physically sound and simpler CI model with a 1 m free space-reference distance term is more convenient to use to model indoor mm-wave channels. Figures 35, 36, 37, and 38 show scatter plots for CI PLM parameters inside modified indoor environments for co-polarized antennas at Tx, 20 LOS, and 122 NLOS readings.
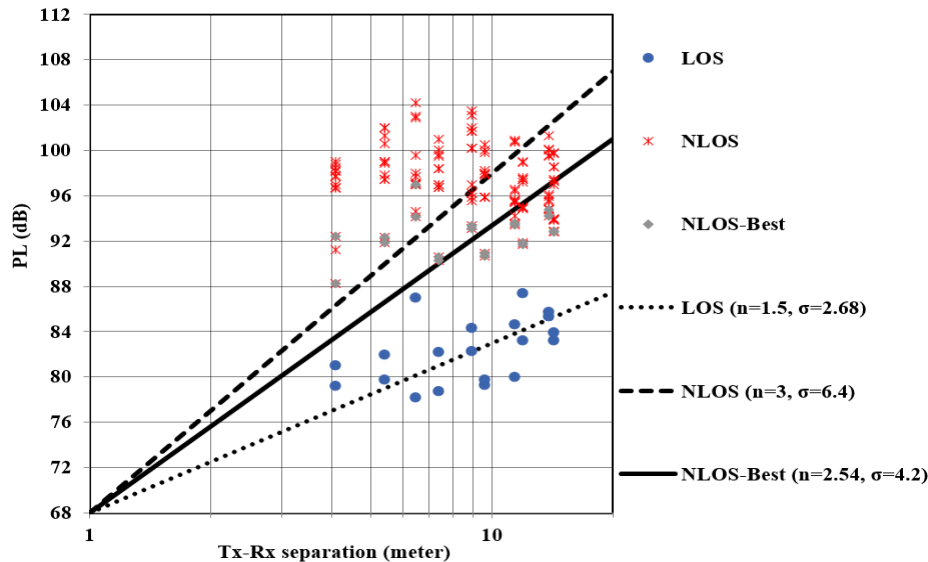
Figure 35. Single-frequency (61.5 GHz) CI ($d_o=1\ m$) PLM parameters scatter plot for Tx at a height of 2.5 m, and Rx antennas height of 1.5 m in an atypical modified indoor office environment (ring FSS wallpaper with humans) for co-polarized antennas
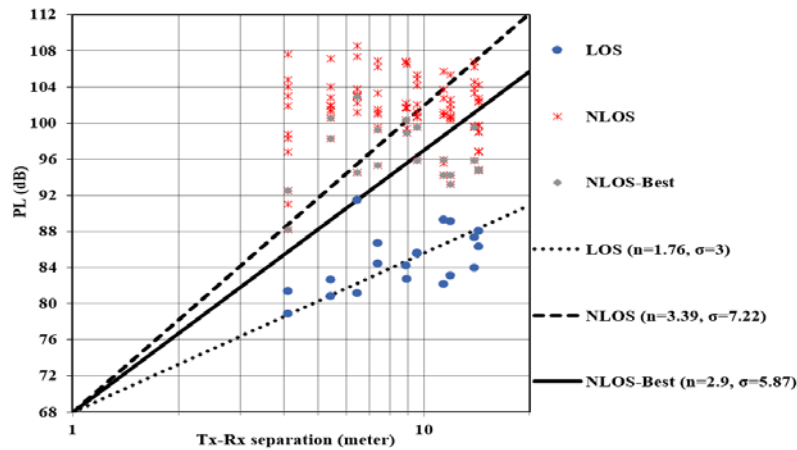
Figure 36. Single-frequency (61.5 GHz) CI (d_o= 1 m) PLM parameters scatter plot for Tx at a height of 2.5 m, and Rx antennas height of 1.5 m in an atypical modified indoor office environment (ring FSS wallpaper without humans) for co-polarized antennas
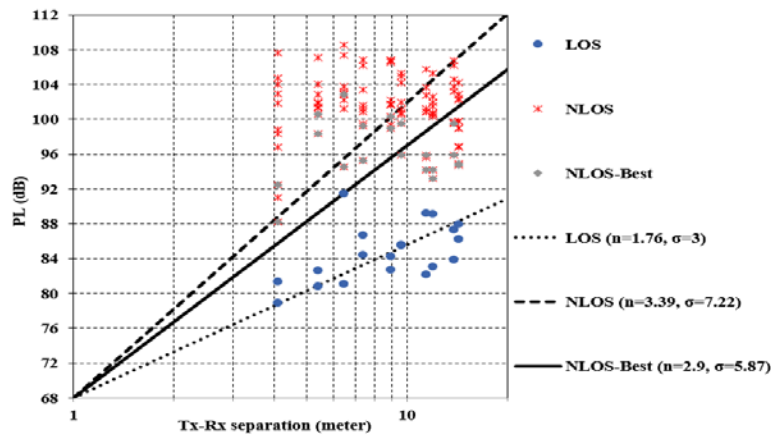
Figure 37. Single-frequency (61.5 GHz) CI (d_o=1 m) PLM parameters scatter plot for Tx at a height of 2.5 m, and Rx antennas height of 1.5 m in an atypical modified indoor office environment (humans without ring FSS wallpaper) for co-polarized antennas
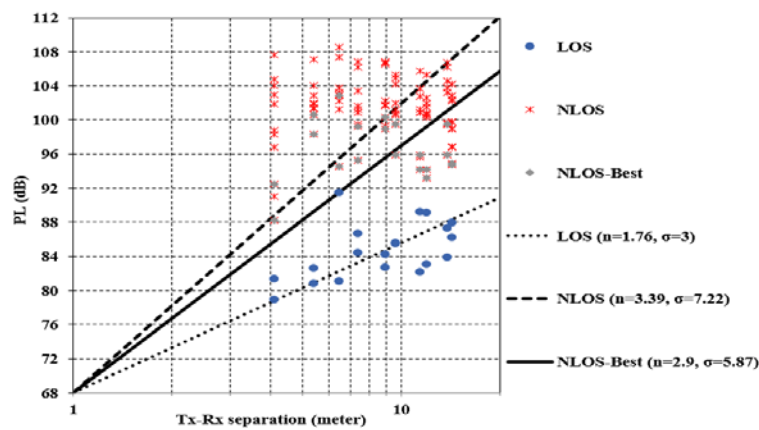
Figure 38. Single-frequency (61.5 GHz) CI (d_o=1 m) PLM parameters scatter plot for Tx at a height of 2.5 m, and Rx antennas height of 1.5 m in an atypical modified indoor office environment (without humans and ring FSS wallpaper) for co-polarized antennas

4.   CONCLUSION

In order to enhance the performance of indoor 60 GHz wireless networks for both SISO and MIMO systems, ring FSS has been selected because the propagation of 60 GHz can be easily blocked by obstacles or humans. Results showed that received signal power had been enhanced by an average of 6.54 and 6.87 dB for SISO and MIMO, respectively. When using MIMO system, the capacity had been enhanced by an average of 24 bit/s/Hz. However, the presence of human bodies attenuated the strength of the received signal power by an average of 2.5 dB, and decreased the capacity by an average of 1.25 bit/s/Hz. While using ring FSS wallpaper, the capacity for MIMO system had been enhanced by an average of 2.5 bit/s/Hz, which proved that the presence of ring FSS wallpaper in an indoor environment increased the strong reflected wave components in each Rx location. Results also showed that the delay spread has been slightly increased after the modification by an average of 7.5 ns, which is still within the acceptable range for a 60 GHz band.

This paper also described mm-wave propagation simulations in modified indoor scenarios at 61.5 GHz and presented and compared the single- frequency FI and CI PLMs. Single-frequency PL results showed that the CI model is preferable to the FI model (presently used in 3GPP) for modified indoor environments due to its physical basis, simplicity, and robustness over measured frequencies and distance ranges.The CI model is physically tied to the transmitter power using a close-in free space reference and standardized measurements around an inherent 1 m free space reference distance that is physically based. Thus, it is easy to use for varying distances since it involves the use of a single parameter (PLE, or n).

REFERENCES

[1]   Alkhawatra, Mohammad, and Nidal Qasem, "Improving and Extending Indoor Connectivity Using Relay Nodes for 60 GHz Applications," *International Journal of Advanced Computer Science & Applications*, vol. 1, no. 7 (2016): 427-434.

[2]   Aldorgham, Emran, Nidal Qasem, and Hadeel Yaseen Alzou'bi, "Overcoming the Influence of Human Shadowing and Obstacles via Modified Building Using Frequency Selective Wallpapers for 60 GHz," *11th Research World International Conference*, Riyadh, Saudi Arabia, (2016) pp. 24-29, ISBN: 978- 93-85973-43-7.

[3]   Ehrig, Marcus, and Markus Petri, "60GHz broadband MAC system design for cable replacement in machine vision applications," *AEU-International Journal of Electronics and Communications*, 67, no. 12 (2013): 1118-1128.

[4]   Maccartney, George R., Theodore S. Rappaport, Shu Sun, and Sijia Deng, "Indoor office wideband millimeter-wave propagation measurements and channel models at 28 and 73 GHz for ultra-dense 5G wireless networks," *IEEE Access*, 3 (2015): 2388-2424.

[5]   Barton, Jay Houston, and Eric Macdonald, "Frequency Selective Surfaces for Exreme Applications," (2014).

[6]   Rafique U, Ali SA, Afzal MT, and Abdin M., "Bandstop filter design for GSM shielding using frequency selective surfaces," *International Journal of Electrical and Computer Engineering*, 2012 Dec 1; 2(6):846.

[7]   Qasem N., "Enhancing wireless communication system performance through modified indoor environments," (Doctoral dissertation, © Nidal Qasem) (2014).

[8]   Wu TK, editor. "Frequency selective surface and grid array," *Wiley-Interscience*; 1995 Jul 31.

[9]   Bharti G, Singh G, Jha KR, Jyoti R., "Circular ring frequency selective surface: a novel synthesis technique," *In Contemporary Computing (IC3)*, 2013 Sixth International Conference on 2013 Aug 8 (pp. 491-496). IEEE.

[10]   Hong JS, Lancaster MJ., "Microstrip filters for RF/microwave applications," *John Wiley & Sons*; 2004 Apr 7.

[11]   CST MICROWAVE STUDIO® - 3D EM Simulation Software [Internet]. Cst.com. 2017 [cited 27 October 2017]. Available from: https://www.cst.com/products/cstmws

[12]   Qasem N, Seager R., "Studies on enhancing wireless signal for indoor propagation," In *Antennas and Propagation Conference (LAPC)*, 2010 Loughborough 2010 Nov 8 (pp. 309-312). IEEE.

[13]   Wireless EM Propagation Software - Wireless InSite [Internet]. Remcom. 2017 [cited 27 October 2017]. Available from: https://www.remcom.com/wireless-insite-em-propagation-software/

[14]   Joshi S, Gupta D, Haque SZ, Kothari N, Bapna PC., "Effect of antenna spacing on the performance of multiple input multiple output LTE downlink in an urban microcell," *International Journal of Wireless & Mobile Networks*. 2012 Dec 1; 4(6):175.

[15]   Dawod D, Qasem N., "Enhancing the capacity of MIMO systems via modified building using Frequency Selective wallpapers," In *Information and Communication Systems (ICICS)*, 2015 6th International Conference on 2015 Apr 7 (pp. 171-176). IEEE.

[16]   Lodro MM, Abro MH., "Ergodic Capacity of MIMO Correlated Channels in Multipath Fading Environment with known Channel State Information," *International Journal of Electrical and Computer Engineering*, 2012 Oct 1;2(5):691.

[17]   Adeogun R., "Capacity and Error Rate Analysis of MIMO Satellite Communication Systems in Fading Scenarios," *International Journal of Electrical and Computer Engineering*, 2014 Aug 9;4(4):614.

[18]   Qasem N, Seager R., "Parametric studies in enhancing indoor wireless communication system via environmental modification," In *Antennas and Propagation Conference (LAPC)*, 2012 Loughborough 2012 Nov 12 (pp. 1-4). IEEE.

[19]   Zhu Y, Zhang Z, Marzi Z, Nelson C, Madhow U, Zhao BY, Zheng H., "Demystifying 60GHz outdoor picocells," In *Proceedings of the 20th annual international conference on Mobile computing and networking* 2014 Sep 7 (pp. 5-16). ACM.

[20] MacCartney GR, Deng S, Rappaport TS., "Indoor office plan environment and layout-based mmWave path loss models for 28 GHz and 73 GHz," In*Vehicular Technology Conference (VTC Spring)*, 2016 IEEE 83rd 2016 May 15 (pp. 1-6). IEEE.

[21] Feuerstein MJ, Blackard KL, Rappaport TS, Seidel SY, Xia HH., "Path loss, delay spread, and outage models as functions of antenna height for microcellular system design," *IEEE Transactions on Vehicular Technology*, 1994 Aug;43(3):487-98.

[22] MacCartney GR, Samimi MK, Rappaport TS., "Omnidirectional path loss models in New York City at 28 GHz and 73 GHz," In *Personal, Indoor, and Mobile Radio Communication (PIMRC)*, 2014 IEEE 25th Annual International Symposium on 2014 Sep 2 (pp. 227-231). IEEE.

[23] Rappaport TS, MacCartney GR, Samimi MK, Sun S., "Wideband millimeter-wave propagation measurements and channel models for future wireless communication system design," *IEEE Transactions on Communications*, 2015 Sep;63(9):3029-56.

[24] Maccartney GR, Rappaport TS, Sun S, Deng S., "Indoor office wideband millimeter-wave propagation measurements and channel models at 28 and 73 GHz for ultra-dense 5G wireless networks," *IEEE Access*, 2015;3:2388-424.

BIOGRAPHY OF AUTHOR

Nidal Qasem received his B.Sc. degree in Electronics and Communications Engineering (Honours) from AL-Ahliyya Amman University, Amman, Jordan, in 2004. He obtained his M.Sc. degree in Digital Communication Systems for Networks & Mobile Applications (DSC) from Loughborough University, Loughborough, United Kingdom, in 2006. He then pursued a PhD degree in wireless and digital communication systems at Loughborough University. He is currently working as an assistant professor in the department of Electronics and Communications Engineering at Al-Ahliyya Amman University. His research interests include propagation control in buildings, specifically improving the received power, FSS measurements and designs, dielectric characterizations of building materials, antennas, ultra-wide band, and wireless system performance analyses.